INTERNATIONAL JOURNAL FOR NUMERICAL METHODS IN FLUIDS
Int. J. Numer. Meth. Fluids 2001; **36**: 287–308 (DOI: 10.1002/fld.133)

Finite element simulations of fully non-linear interaction between vertical cylinders and steep waves. Part 2: Numerical results and validation

Q. W. Ma[a,*], G. X. Wu[a] and R. Eatock Taylor[b]

[a] *Department of Mechanical Engineering, University College London, Torrington Place, London, U.K.*
[b] *Department of Engineering Science, University of Oxford, Parks Road, Oxford, U.K.*

SUMMARY

In Ma, Wu, Eatock Taylor [Finite element simulation of fully non-linear interaction between vertical cylinders and steep waves. Part 1: methodology and numerical procedure. *International Journal for Numerical Methods in Fluids* 2001], designated Part 1 hereafter, we have developed the methodology and solution procedure for simulating the three-dimensional interaction between fixed bodies and steep waves based on a finite element method (FEM). This paper provides extensive numerical results and validation. The effectiveness of the radiation condition is investigated by comparing the results from short and long tanks; the accuracy of the computed data is confirmed through comparison with analytical solutions. The adopted mathematical model is also validated by comparing the obtained numerical results with experimental data. Various test cases, including non-linear bichromatic and irregular waves and the interactions between waves and one or two cylinders, are analysed. Copyright © 2001 John Wiley & Sons, Ltd.

KEY WORDS: finite element method; non-linear interaction; numerical tank; steep waves; vertical cylinders

1. INTRODUCTION

As described in Part 1 [1], the present analysis uses a time marching technique based on fully non-linear potential theory and tackles the three-dimensional boundary value problem at each time step using a finite element method (FEM). The algebraic equations resulting from the FEM are solved by a conjugate gradient iterative method with a symmetric successive overrelaxation (SSOR) pre-conditioner, including a carefully selected parameter. A post-processor based on the recovery technique is adopted in order to improve the accuracy of the

* Correspondence to: Department of Mechanical Engineering, University College London, Torrington Place, London WC1E 7JE, U.K.

Received June 1999
Revised November 1999

finite element solution without increasing the number of elements. A radiation condition is imposed on the truncated boundary, which is based on the combination of a damping zone and a Sommerfeld condition.

The present paper gives extensive numerical results and validation. The following sections start with the optimization of parameter ν_0 used in the damping zone (see Section 2.2 of Part 1 for details [1]). The numerical results for both regular and irregular waves with different amplitudes are then provided. Extensive results are presented for interactions between steep waves and one or two cylinders. The computed results are compared with analytical solutions and experimental data for some cases and agreement is found to be satisfactory.

In the analysis carried out below, d, $\sqrt{d/g}$ and ρ are used as the basic parameters for non-dimensionalization. In particular, the following parameters are defined by:

$$(x, y, z, \zeta, L, B, a, R_0, \lambda) \to (x, y, z, \zeta, L, B, a, R_0, \lambda)d, \; t \to \tau\sqrt{\frac{d}{g}}, \quad \omega \to \omega\sqrt{\frac{g}{d}}, \quad k \to \frac{k}{d},$$
$$F \to F\rho g d^3, \quad M \to M\rho g d^4 \tag{1}$$

Most of these definitions can be found in Part 1 (figure 1) and Equations (1), (7), (12), (13) and (22). In addition, a will be used as the amplitude of wave-maker motion and R_0 is the radius of the cylinder placed in the tank.

2. WAVES GENERATED IN THE NUMERICAL TANK

The numerical simulation of wave propagation in a tank without any cylinder is investigated first. The generated waves may be monochromatic, bichromatic or irregular. Figure 1 shows an illustration of a coarse mesh used at the start of a typical calculation.

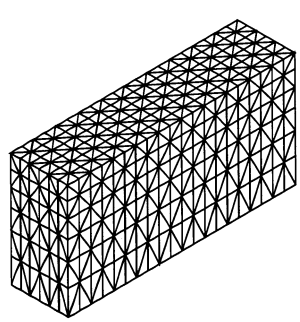

Figure 1. Typical initial coarse mesh for the wave-maker problem.

2.1. Optimization of the parameter v_0 in the damping zone

Section 2.2 of Part 1 outlines the procedure through which the radiation condition is imposed. It is done by a combination of the Sommerfeld condition and a damping zone. The damping zone is applied over a length L_{dm} specified in that section. Here the way to choose the other parameter v_0 in the damping zone will be discussed. This parameter is optimized using numerical tests as follows. In these tests, the efficiency of absorption is measured by an absorption coefficient, C_{a}, defined by

$$C_{\mathrm{a}} = 1 - \frac{\Delta A_{\mathrm{r}}}{A_0} \tag{2}$$

where A_0 is the amplitude of the incident wave without reflection and ΔA_{r} is the amplitude of the reflected wave. If there is no reflection, i.e. $\Delta A_{\mathrm{r}} = 0$, then $C_{\mathrm{a}} = 1$; on the other hand if the wave is completely reflected, $C_{\mathrm{a}} = 0$.

Neither A_0 nor ΔA_{r} is available prior to the simulation and both have to the determined numerically. ΔA_{r} is estimated from $\Delta A_{\mathrm{r}} = |A_0 - A_{\mathrm{r}}|$, where A_{r} is the total amplitude of the wave including the reflection. A_{r} is obtained from the envelope of the wave history recorded at point $x = (L/2) - (L_{\mathrm{dm}} + 0.2\lambda)$, which is situated just upstream of the left edge of the damping zone. A_0 is approximated by the amplitude of the wave generated under the same conditions but in a longer tank, recorded at the same point as that for A_{r}.

In order to find the optimum value of v_0, waves are generated by the piston wave-maker undergoing the following motion:

$$S(\tau) = -a\cos(\omega\tau) \tag{3}$$

$$U(\tau) = a\omega\sin(\omega\tau) \tag{4}$$

where $S(\tau)$ is the displacement of the wave-maker, a is its amplitude and $U(\tau)$ is its velocity. The frequency ω of the motion is taken in the range 0.5–3.0. In the shorter tank, the initial distance between the wave-maker and the left edge of the damping zone is set at about 4λ, and this distance in the longer tank is about 12λ. The calculation is made over about 14 periods. The corresponding amplitudes of the wave-maker are specified in such a way that all the resulting waves have steepness $\varepsilon = H/\lambda \approx 0.005$, where H is the wave height.

Figure 2(a) shows the absorption coefficient against frequency ω and parameter v_0. For each frequency, one can find a maximum absorption coefficient from this figure, as shown in Figure 2(b). The values of v_0 corresponding to each of the maximum absorption coefficients are then determined for every frequency. These values are plotted against the frequency as stars in Figure 3. The discrete numerical values can be fitted by a third-order polynomial

$$v_0 = 0.0496\omega^3 - 0.1751\omega^2 + 0.2352\omega - 0.0689 \tag{5}$$

which is illustrated as the solid line in Figure 3. This equation provides a convenient way of implementing the damping zone and allows us to set up the radiation condition in the computer program by choosing parameter v_0 automatically once the frequency is specified.

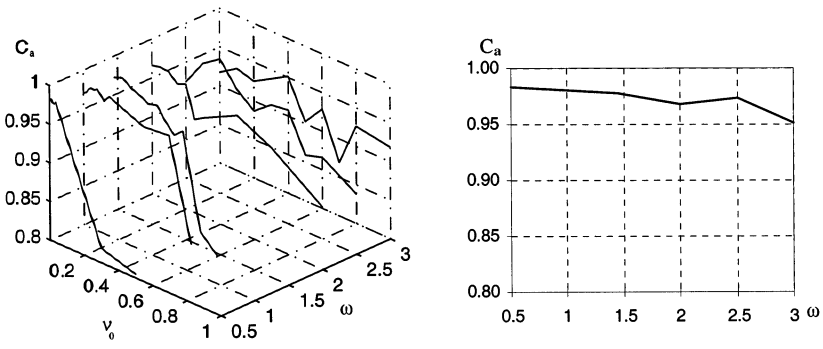

(a) C_a via ω and v_0 (b) Maximum C_a via ω

Figure 2. Absorption coefficient for different ω and v_0.

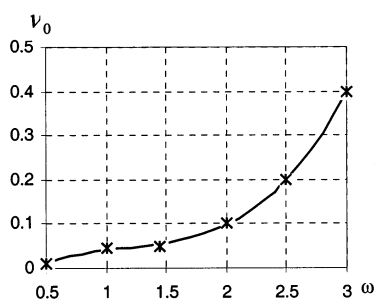

Figure 3. Optimum v_0 against ω.

As shown in Figure 2(b), the absorption coefficient can be very close to unity if parameter v_0 is determined by Equation (5). However, Equation (5) has been obtained by numerical tests on waves with low steepness. In order to check if it is suitable for waves of greater steepness, cases with various values of ε are also simulated. For each of these cases, the frequency is kept constant. Figure 4 plots the obtained absorption coefficients. It can be seen that the absorbing efficiency is still very good even when the wave steepness is 0.08 (under ideal conditions, the maximum steepness for a Stokes wave is about 0.14, but in some numerical simulation the maximum achievable steepness may be reduced to 0.1 [2]). The efficiency does, however, decrease slightly with increase in the steepness.

2.2. Comparison with the analytical solution

For a wave having very small steepness, a linearized analytical solution may be found (e.g. Reference [3]). This solution can be used as a check on the numerical method. For a particular

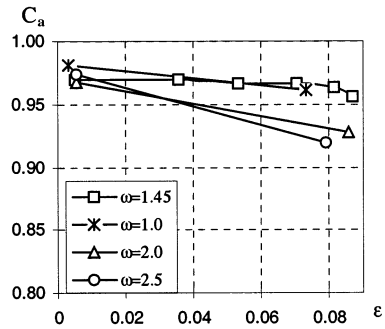

Figure 4. Absorption coefficient against wave steepness (v_0 evaluated by Equation (5)).

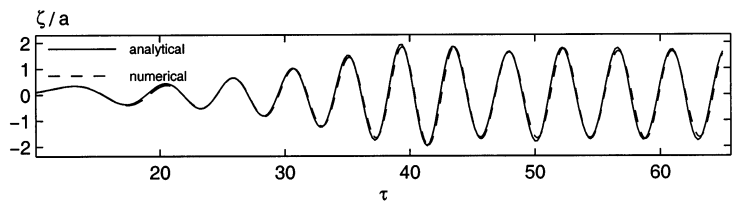

Figure 5. Comparison of the wave history with the analytical solution at $x \approx 3.74$ for the case with $\omega = 1.45$ and $a = 0.0041$.

case in a tank having the length of $L \approx 15$, the numerical and analytical results for the time history of wave elevation at $x \approx 3.74$ are shown in Figure 5. In Figure 6 the profiles at two instants are plotted for the same case. In Figure 6(a) the steady state wave has not yet reached the damping zone, whereas it has in Figure 6(b). The figures show that the numerical results are in very good agreement with the corresponding analytical solutions; although the difference in the profiles is slightly greater within the damping zone, as is expected. The cases with other frequencies and amplitudes used in the damping zone investigation have also been compared with the analytical solution. The results for all of them show a similar agreement with the analytical solution to that seen in these two figures.

2.3. Waves with larger amplitudes

Waves with various frequencies and larger amplitudes were also simulated. One example of a time history is shown in Figure 7. It can be seen from these plots that the waves with larger amplitudes have flatter troughs and sharper crests. In addition, it is observed that the waves with larger amplitudes travel faster and have longer wavelengths than those with smaller amplitudes. The same phenomenon has also been noted in other cases with different frequencies. This phenomenon for the transient wave is similar to the so-called amplitude dispersion of Stokes waves, as discussed, for example, by Newman [4].

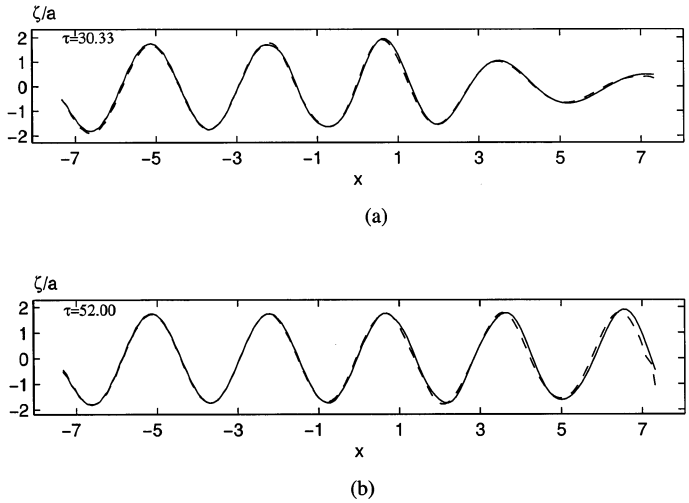

Figure 6. Comparison of the wave profiles with the analytical solution for the case with $\omega = 1.45$ and $a = 0.0041$. The damping zone begins at $x_d = 4.32$ (solid line: analytical solution; dashed line: numerical results). Results shown for (a) $\tau = 30.33$; (b) $\tau = 52.00$.

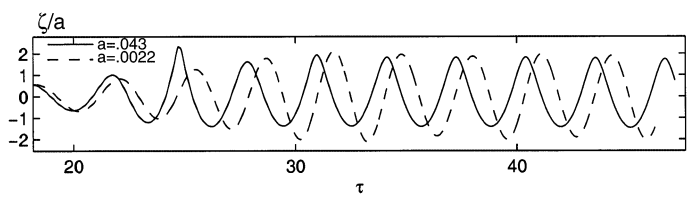

Figure 7. Wave history for different amplitudes ($L = 9.28$; $\omega = 2.0$; recorded at $x = 1.33$).

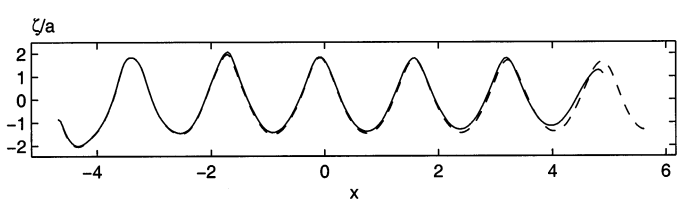

Figure 8. Wave profiles at $\tau = 15T$ ($= 2\pi/\omega$) for different lengths of tank ($\omega = 2.0$, $a = 0.043$; damping zone of shorter tank beginning at $x_d = 1.64$; solid line: shorter tank $L = 9.28$; dashed line: longer tank $L = 25.28$).

To show how the radiation condition works in the above cases with greater steepness, Figure 8 provides a comparison of wave profiles obtained from tanks of different lengths. For this, the steepness is estimated as $\varepsilon \approx 0.085$. It is shown that the results from shorter and longer tanks are in very good agreement at the centre of the tank, which implies that the reflection is still not significant in the shorter tank.

2.4. Bichromatic waves

The motion of the wave-maker in this case consists of two components and is give by

$$S(\tau) = -a_1 \cos(\omega_1 \tau) - a_2 \cos(\omega_2 \tau) \tag{6}$$

where $S(\tau)$ is the displacement of the wave-maker as before; a_1 and a_2 are the amplitudes corresponding to the components of frequency ω_1 and ω_2 respectively. The corresponding velocity then becomes

$$U(\tau) = a_1 \omega_1 \sin(\omega_1 \tau) + a_2 \omega_2 \sin(\omega_2 \tau) \tag{7}$$

The parameters in the radiation condition described above have been chosen for monochromatic waves. In order to use Equation (5) for bichromatic waves, the first task is obviously to choose a suitable frequency that determines v_0 and c. A suggestion is given below

$$\omega = \begin{cases} \omega_1, & a_1 > a_2 \\ \omega_2, & a_2 > a_1 \end{cases} \tag{8}$$

Based on this, several cases with various combinations of frequencies and amplitudes have been calculated. Figure 9 shows the wave history for one of the cases while Figure 10 illustrates the corresponding wave profiles along the tank. It can be seen that results corresponding to tanks of different length are in good agreement.

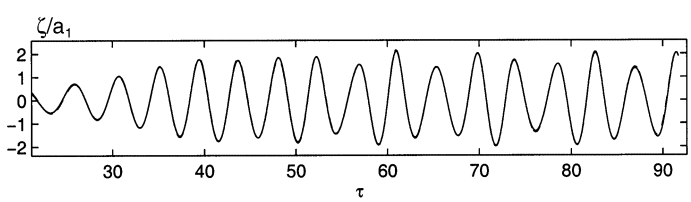

Figure 9. Wave history recorded at $x \approx 3.74$ ($a_1 = 0.016$, $\omega_1 = 1.45$; $a_2 = 0.2a_1$, $\omega_2 = 2.03$; damping zone in the shorter tank beginning at $x_d = 4.32$; solid line: shorter tank $L = 14.64$; dashed line: longer tank $L = 44.64$).

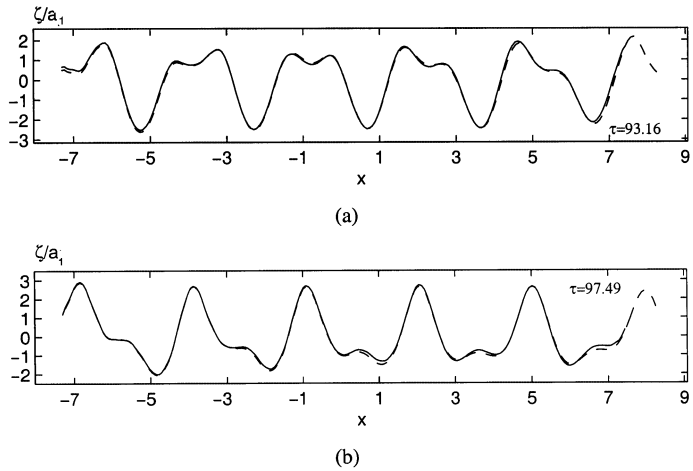

Figure 10. Wave profiles at different time instants ($a_1 = 0.016$, $\omega_1 = 1.45$; $a_2 = 0.5a_1$, $\omega_2 = 2.03$; damping zone in the shorter tank beginning at $x_d = 4.32$; solid line: shorter tank $L = 14.64$; dashed line: longer tank $L = 44.64$). Results shown for (a) $\tau = 93.16$; (b) $\tau = 97.49$.

2.5. Irregular waves and comparison with some experimental results

In irregular waves a rational choice for the frequency ω in the radiation condition would seem to be that corresponding to the maximum value of the wave spectrum. A test case has been investigated in which the irregular wave is generated by a wave-maker subject to the time history of displacement obtained by scaling the data in Figure 11 by $\alpha = 0.612$, as given by Nestegard [5]. Fourier analysis performed on these data shows that the dimensionless frequency corresponding to the maximum of the wave spectrum is about 1.20, which is chosen for ω in the radiation condition. Figure 12 plots the profiles of wave elevations at different time steps and demonstrates that the wave has obviously died away in the tank. This implies that the waves are transmitted through the far end with little reflection, and the effectiveness of the radiation condition is maintained for this case.

Figure 13 shows the wave histories recorded at $x = 3.436$, together with some experimental data provided by Nestegard [5] for comparison. A similar comparison is also made in Figure

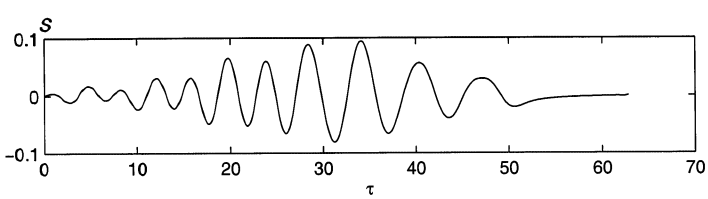

Figure 11. The displacement of the wave-maker generating irregular wave (set to be at rest after $\tau \approx 58$).

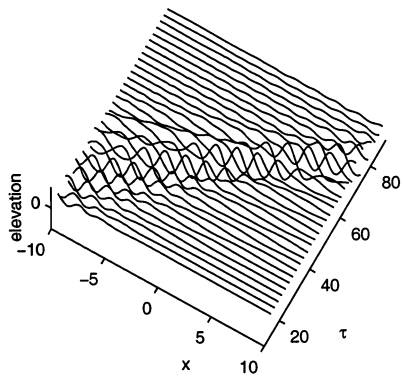

Figure 12. Irregular wave profiles at different time steps.

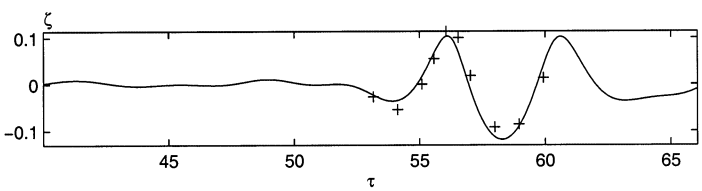

Figure 13. The history of an irregular wave recorded at $x = 3.436$ for $\alpha = 0.612$ (solid line: shorter tank; dashed line: longer tank; damping zone beginning at $x_d = 7.0$; $+$: experimental data from Nestegard [5]).

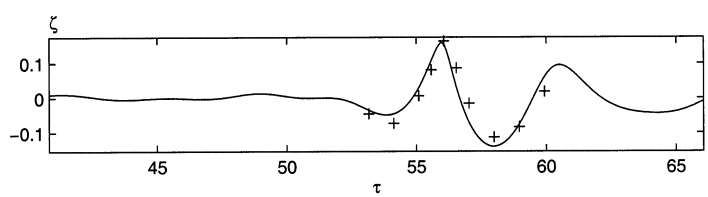

Figure 14. The history of an irregular wave recorded at $x = 3.436$ for $\alpha = 0.749$ (solid line: shorter tank; damping zone beginning at $x_d = 7.0$; $+$: experimental data from Nestegard [5]).

14 for a case where a steeper wave is generated by the wave-maker, its displacement time history being obtained by scaling the data in Figure 11 by a larger factor ($\alpha = 0.749$). Both figures show that the numerical results agree well with the experimental data.

It should be noted that the accuracy of the numerical results could be affected by the frequency of remeshing. For the results from our calculations reported by Nestegard [5], the agreement with experimental data is not as good as in this paper, as remeshing was applied

there at each time step. This led to loss of energy due to numerical damping. Since those results submitted in 1997, further improvements have been made, by reducing the frequency of remeshing based on a compromise between avoiding overly distorted meshes and reducing the loss of energy. More importantly, the recovery technique has been implemented here. These improvements have led to a better agreement in Figures 13 and 14, as well as in Figure 22 of the next section.

The calculation has also been undertaken for the case presented by Clauss and Steinhagen [6]. The tank length is taken as $L = 49.9$ and the frequency used for the radiation condition is taken as $\omega = 0.6$. This displacement of the wave-maker and corresponding wave histories at two different positions are plotted in Figure 15. The numerical results are in excellent agreement with the experimental results of Clauss and Steinhagen [6], which are represented by the dashed line. Even at a large distance from the wave-maker, the high waves are well predicted.

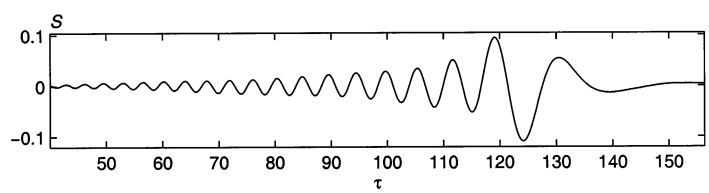

(a) displacement of wave-maker

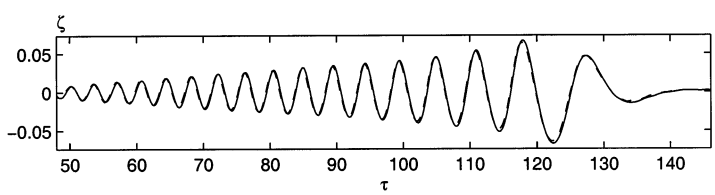

(b) wave history at $x = 0.895$

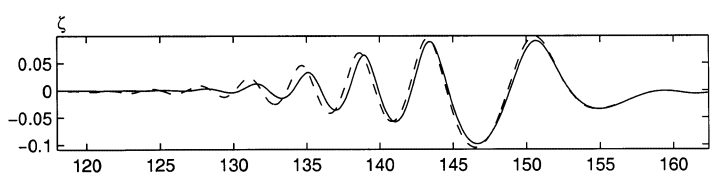

(c) wave history at $x = 22.52$

Figure 15. Comparison of wave history with the experimental results of Clauss and Steinhagen [6] (solid line: numerical; dashed line: experimental).

3. ONE VERTICAL CYLINDER

The second case considered is the interaction between waves and one vertical cylinder in the tank (a sketch of the problem is shown in figure 1 of Part 1 [1]). The radiation condition is imposed at the far end of the tank. It should be noted that the waves transmitted past the cylinder are three-dimensional. Although the damping zone may also be applicable for three-dimensional waves, the Sommerfeld condition implemented is suitable for two-dimensional waves as the phase velocity of the wave and the moving velocity of the truncated boundary are assumed to be constant across the tank. Tests have shown that the non-uniformity of these parameters does not affect the results presented below (see Reference [7] for details).

Meshes used in the simulation are similar to, although finer than, that in Figure 1, and in the subdomain around the cylinder, the two vertical planes are now radial and circumferential. The plan form of a typical mesh is shown in Figure 16.

Figure 17 gives the time history of the force acting on the cylinder in the x-direction, when it is subjected to monochromatic waves generated at the frequency $\omega = 2.0$ and three different amplitudes. The non-dimensionalized force is divided by the term $R_0^2 a$. Here the radius of the cylinder is $R_0 = 0.1416$ while the tank width, B, is 0.62. It can be seen that the non-linear effect is visible at large amplitude, i.e. the crest is larger than the trough in the force history when

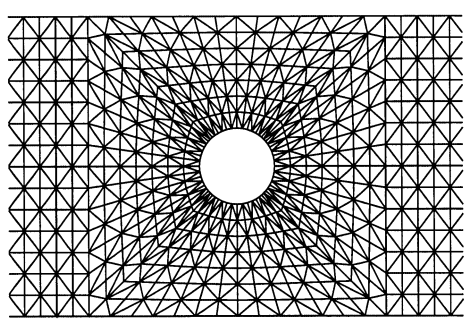

Figure 16. Mesh around a cylinder.

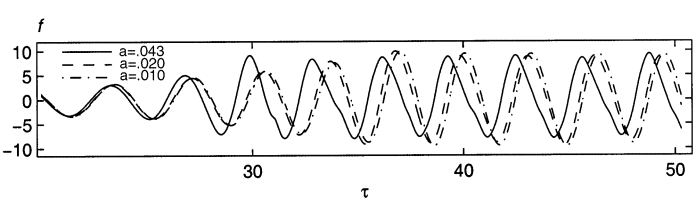

Figure 17. Forces for different amplitudes of the wave-maker ($R_0 = 0.1416$, $B = 0.62$, $L_{wc} = 7.0$, $L_{cd} = 5.0$, $\omega = 2.0$; $f = F_x/R_0^2 a$).

the wave is steeper. In addition, the transient period of the force history corresponding to the steeper wave becomes shorter. This implies that the steeper wave travels faster, reflecting the amplitude dispersion due to non-linearity, as discussed in Section 2.3. To further illustrate the non-linear behaviour of the wave force, Fourier analysis of the time history of the force has been performed over the near-steady state range shown in Figure 17. The non-linear contribution is obtained by subtracting the first harmonic component from the total force. Figure 18 gives the estimated non-linear contribution, f_h, as well as the corresponding total force for the three cases given in Figure 17 plotted over the range $36 < \tau < 49$. These figures suggest that the non-linear contributions become more important with increase of the amplitude of the wave-maker. Further work is required to extract more detailed information about the non-linear behaviour.

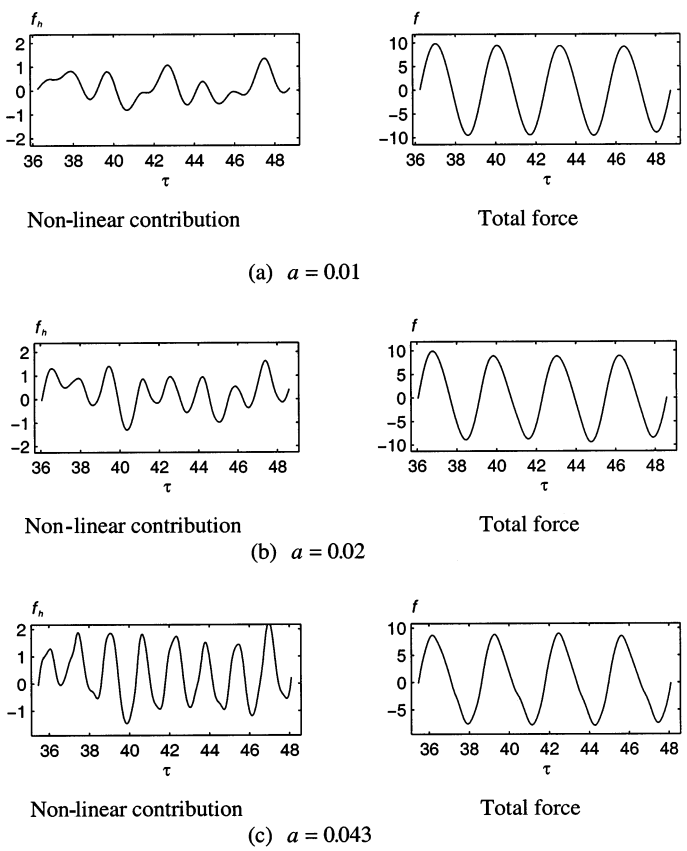

Figure 18. Non-linear contributions to the force obtained by Fourier analysis ($R_0 = 0.1416$, $B = 0.62$, $L_{wc} = 7.0$, $L_{cd} = 5.0$, $\omega = 2.0$; $f = F_x/R_0^2 a$).

The corresponding run-up on the front side of the cylinder is shown in Figure 19. The run-up profiles around the cylinder at different time steps are illustrated in Figure 20 for the cases with $a = 0.01$ and $a = 0.043$. To demonstrate the behaviour of the profiles in three dimensions, some 'snapshots' of the free surface elevation around the cylinder are presented in Figure 21. Very different behaviours at the different amplitudes are demonstrated in these figures. In particular, in Figure 20(b) and Figure 21, quite steep wave profiles appear, which are more or less similar to the bores in shallow water waves. Stansberg [8] provided some

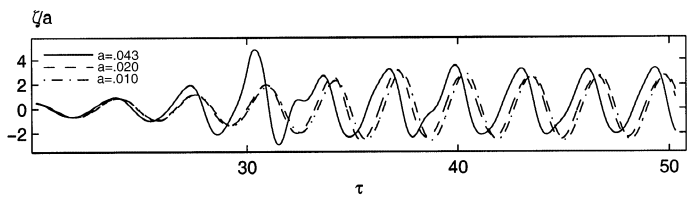

Figure 19. The time history of wave run-up on the front side of the cylinder surface for different amplitudes of the wave-maker ($R_0 = 0.1416$, $B = 0.62$, $L_{wc} = 7.0$, $L_{cd} = 5.0$, $\omega = 2.0$).

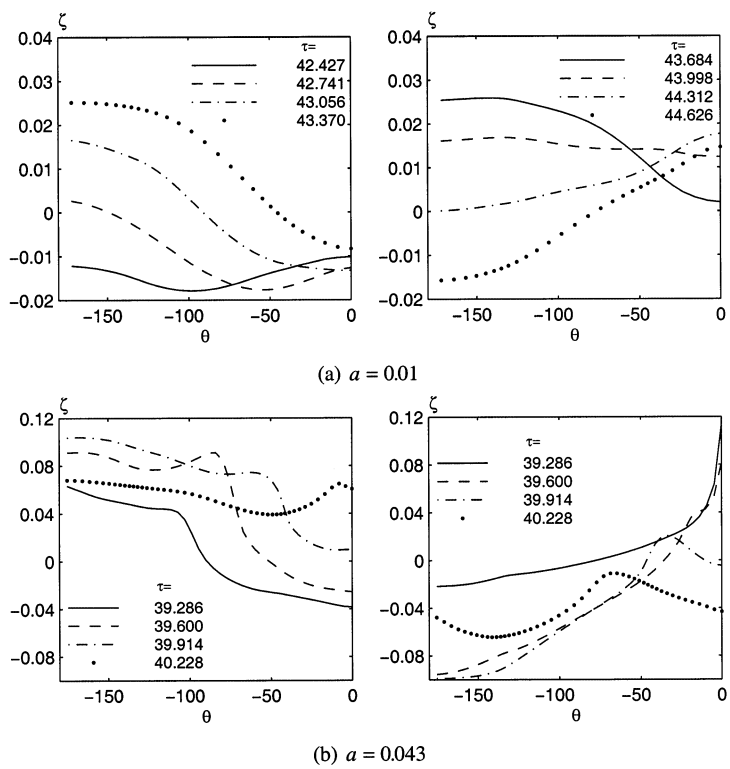

Figure 20. Wave profiles on the waterline of the cylinder at different time steps ($\omega = 2.0$).

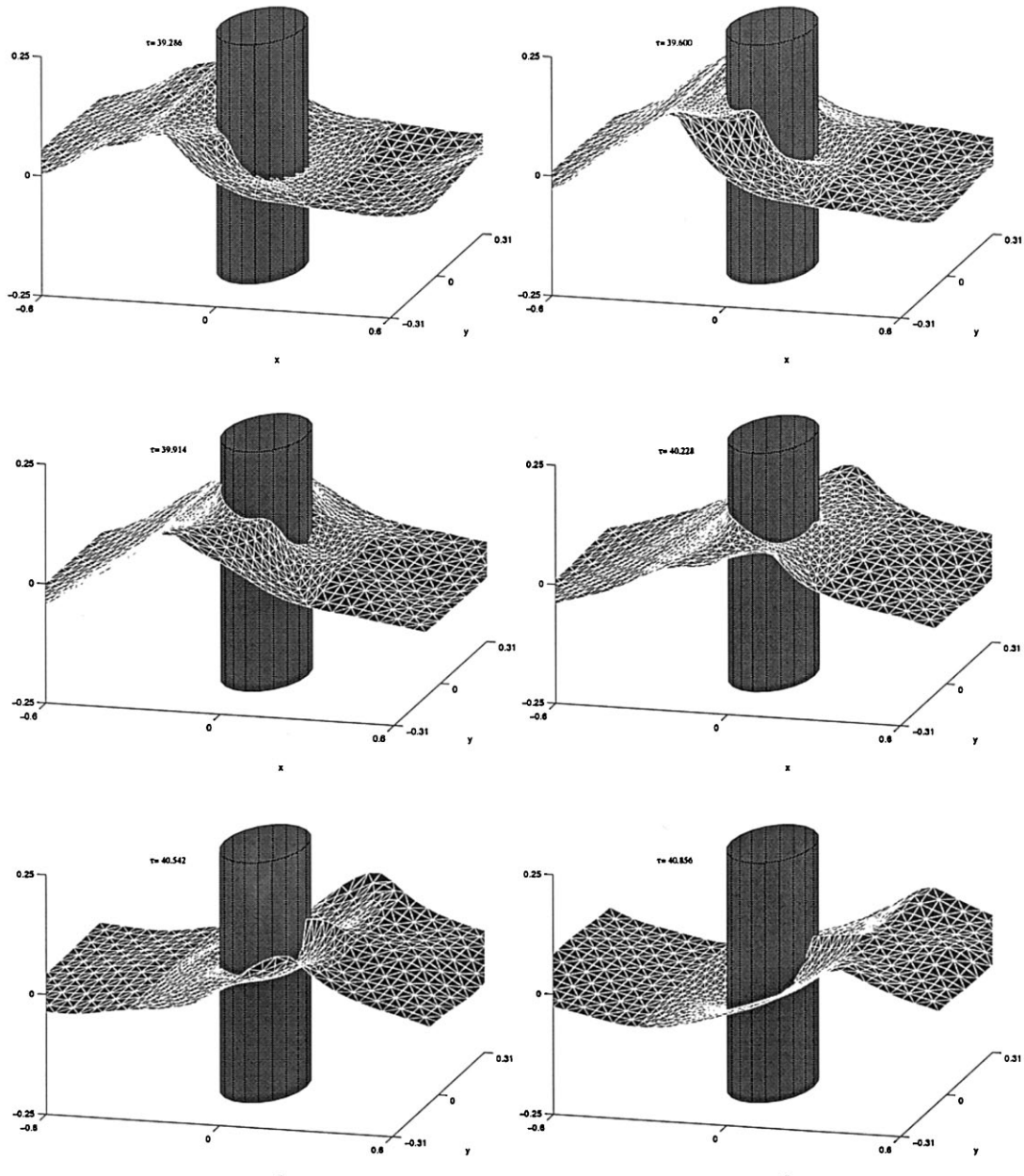

Figure 21. Snapshots of wave profiles around the cylinder ($\omega = 2.0$ and $a = 0.043$). Label for x-axis: -0.6, 0, 0.6; for y-axis: -0.31, 0, 0.31; for vertical axis: -0.25, 0, 0.25.

figures showing the local behaviour as a wave passes a cylinder, based on this experimental data. The wave patterns in his figures are very similar to those at $\tau = 39.286$ and $\tau = 39.914$ in Figure 20(b). Krokstad and Stansberg [9] also reported observing some bore-like waves (named 'hydraulic jumps' in their work) around the cylinder during their experiments. Precise comparison with their work is difficult since the information they gave is not sufficient for us to generate identical waves. Nevertheless, there is a considerable degree of similarity between our numerical simulation and their experimental results.

The interaction between one cylinder and the two irregular waves shown in Figures 12 and 14 has been investigated. The cylinder is the same as above, but the parameters for the tank are now taken as $B = 1.119$, $L_{wc} \approx 13.44$ and $L_{cd} \approx 8.56$ respectively. The numerical results are compared with the experimental measurements for the force in the x-direction in Figure 22, where the non-dimensionalized force is divided by R_0^3 to be consistent with that in Nestegard [5]. It can be seen that the agreement is quite good.

4. TWO VERTICAL CYLINDERS

We now consider two vertical circular cylinders in the tank with their centres on a line parallel to the direction of wave propagation. The problem can be considered as equivalent to four-cylinders in head seas, if the symmetry plane is taken as one of the sidewalls of the tank. This two-cylinder problem is, therefore, of considerable practical interest. The main difference between the problems of one and two cylinders is that in the latter case, one cylinder is in the diffracted wave field of the other. There have been several published linear analyses of the multiple scattering phenomena (e.g. Reference [10]). The second-order problem, including the behaviour of the free surface near the cylinders, has recently been analysed by Malenica *et al.* [11]. However, there are no published results for multiple cylinders based on the fully non-linear theory.

The linearized analytical solution for multiple cylinders in the open sea has been presented by McIver and Evans [10] and by Spring and Monkmeyer [12]. In particular, the latter paper

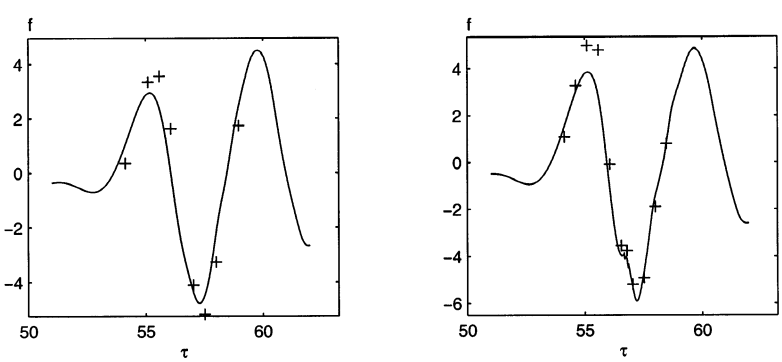

(a) $\alpha = 0.612$ (b) $\alpha = 0.749$

Figure 22. Forces acting on a cylinder subjected to irregular waves ($R_0 = 0.1416$, $B = 1.119$, $L_{wc} \approx 13.44$, $L_{cd} \approx 8.56$; $+$: experimental data from Nestegard [5], $f = F_x/R_0^3$).

gave various results for two cylinders. That solution is used here for comparison with our numerical results. To do so, a Fourier analysis is performed on the time history of the force from the fully non-linear analysis when it has reached the periodic state, to obtain the first harmonic component. According to the examples presented by McIver and Evans [10], the force on the upstream (first) cylinder is clearly affected by the presence of the downstream (second) cylinder, while the influence of the first cylinder on the second is almost negligible when $kl \geq 2$ (where l is the distance between the centres of the cylinders). Therefore, the following comparison is make for the first cylinder only.

The first harmonic components from the numerical results and the linear analytical solutions are compared for different values of kl in Figure 23. In this figure, $X_1 = F_{x1}/F_x$ is the ratio of the force (F_{x1}) in the x-direction on the first cylinder to the same force (F_x) on a single cylinder. This figure shows that the results agree well with the analytical solution, although some difference is visible. It should be noticed that the solid line corresponds to the force in the open sea, and thus some of the differences may result from the sidewall effects of the tank. A body of work has been devoted to the sidewall effects. One example is the paper by Linton and McIver [13], who used the multi-pole method and presented analytical results for the force on two cylinders against different values of $kB/2\pi$ for $2R_0/B = 1/12$ and $2l/B = 0.5$. They carried out some additional calculations and provided us with the results for the case we have investigated here. These are plotted in Figure 23 as triangles. Our numerical results are generally closer to the solution of Linton and McIver [13] for the cylinder in the tank than to the open sea results.

In Figure 24, the time histories of the force $f = F_x/R_0^2 a$ and moment $f_m = M_y/R_0^2 a$ on the two cylinders are illustrated for the case with $kl = 2$. The moment M_y is taken about the bottom of each cylinder. It can be seen that the shapes of the curves of the moment history are very similar to those of the force history. It is also seen that the amplitude of the force and moment on the first cylinder is slightly larger (about 10 per cent) than that on the second one in this case. Figure 25 illustrates the passage of the wave past the cylinders for this case of small wave amplitude ($a = 0.004$).

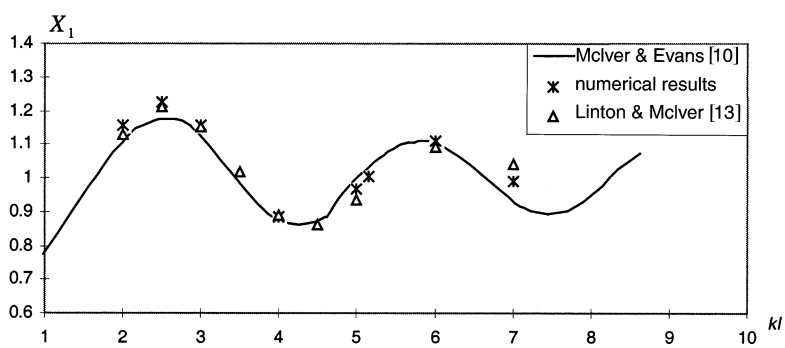

Figure 23. Comparison of the numerical force on the first cylinder with the analytical solutions ($\omega = 16748$, $a = 0.004$, $R_0 = 0.1416$, $B = 2.832$, two cylinders at the centreline of the tank).

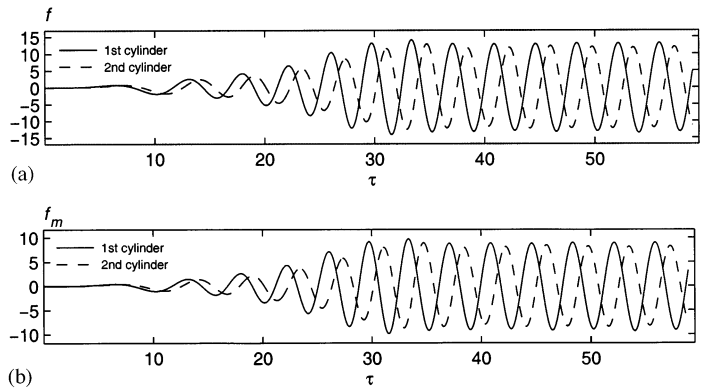

Figure 24. The time history of force and moment on two cylinders ($kl = 2$, $\omega = 1.6748$, $a = 0.004$, $R_0 = 0.1416$, $B = 2.832$): (a) forces ($f = F_x/R_0^2 a$); (b) moments ($f_m = M_y/R_0^2 a$).

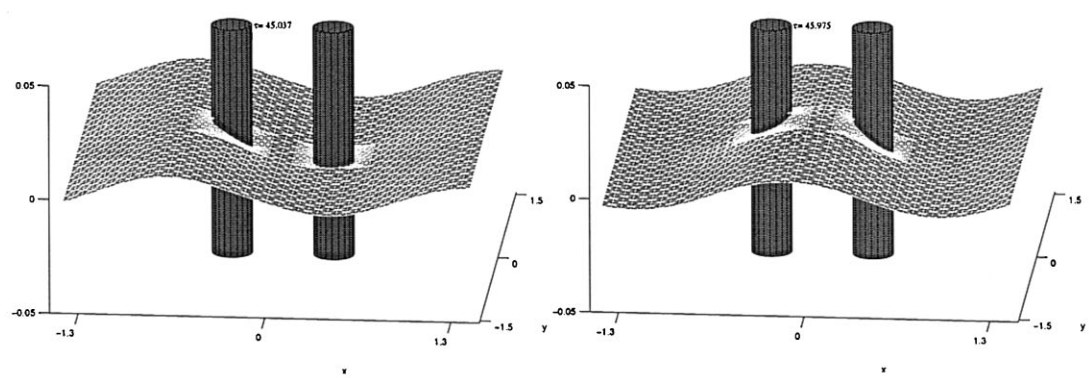

Figure 25. Snapshots of the wave profiles around the two cylinders ($kl = 2$, $\omega = 1.6748$, $a = 0.004$, $R_0 = 0.1416$, $B = 2.832$). Label for x-axis: -1.3, 0, 1.3; for y-axis: -1.5, 0, 1.5; for vertical axis: -0.05, 0, 0.05.

We also calculated some cases with similar frequencies but larger amplitudes. One of the examples corresponds to $a = 0.035$. The time histories of the force and the run-up on the front sides of the cylinder surfaces for this case are given in Figures 26 and 27. The corresponding snapshots in one period are shown in Figure 28. From the run-up history and snapshots, it can be seen that short local waves also appear as in the single cylinder case shown in Figure 21. In order to illustrate the influence of the interaction between the two cylinders on the local waves, Figure 29 presents the corresponding wave profiles around a single cylinder. All wave parameters and tank dimensions for Figures 28 and 29 are identical. These figures clearly show that the local waves become more apparent due to the presence of the interaction between the two cylinders. This influence should also be reflected in the force, moment and run-ups. To

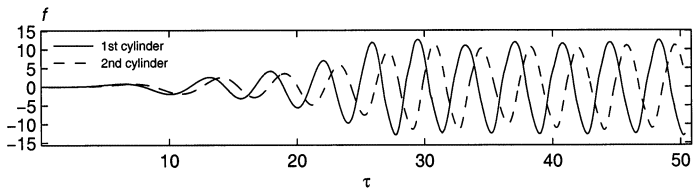

Figure 26. The time history of the forces on two cylinders ($kl = 2$, $\omega = 1.6748$, $a = 0.0035$, $R_0 = 0.1416$, $B = 1.416$).

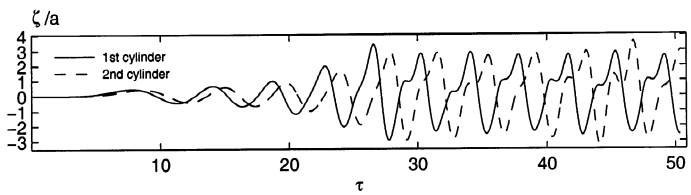

Figure 27. The time history of the run-up on front side of cylinder surfaces ($kl = 2$, $\omega = 1.6748$, $a = 0.0035$, $R_0 = 0.1416$, $B = 1.416$).

illustrate this, the estimated non-linear components of the force are shown in Figure 30 for the single cylinder and for the first cylinder in the two-cylinder problem. The results suggest that the non-linear effects become substantially larger due to the interaction between the cylinders.

Figure 31 illustrates the wave profiles for a case similar to that in Figure 28. Almost all the parameters are the same in the two figures. The only difference is that the two cylinders in this figure are closer to the wall at $y = B/2$, with the distance to the wall from the center of the cylinders being $l_y \approx 0.3B$, while they are situated at the centre in Figure 28. This figure shows that the interactions in the off-case are considerably more complex than those evident in Figure 28. It should also be noted that because the value of l_y can be arbitrarily specified; this case also demonstrates the potential of the presented methodology for dealing with four-legged platforms in head seas in the tank. In such cases, the centreline of the four-legged structure can be used as a sidewall, and symmetry used to represent the problem by just two cylinders in the tank.

5. CONCLUSION

In this paper, which comprises Part 2 of this work, the methodology and the corresponding numerical procedure described in Part 1, based on a three-dimensional FEM, have been used to simulate steep waves and their interaction with vertical cylinders. The numerical results have been compared with those obtained by analytical solutions and experimental data. All have shown that the numerical calculation can give satisfactory results.

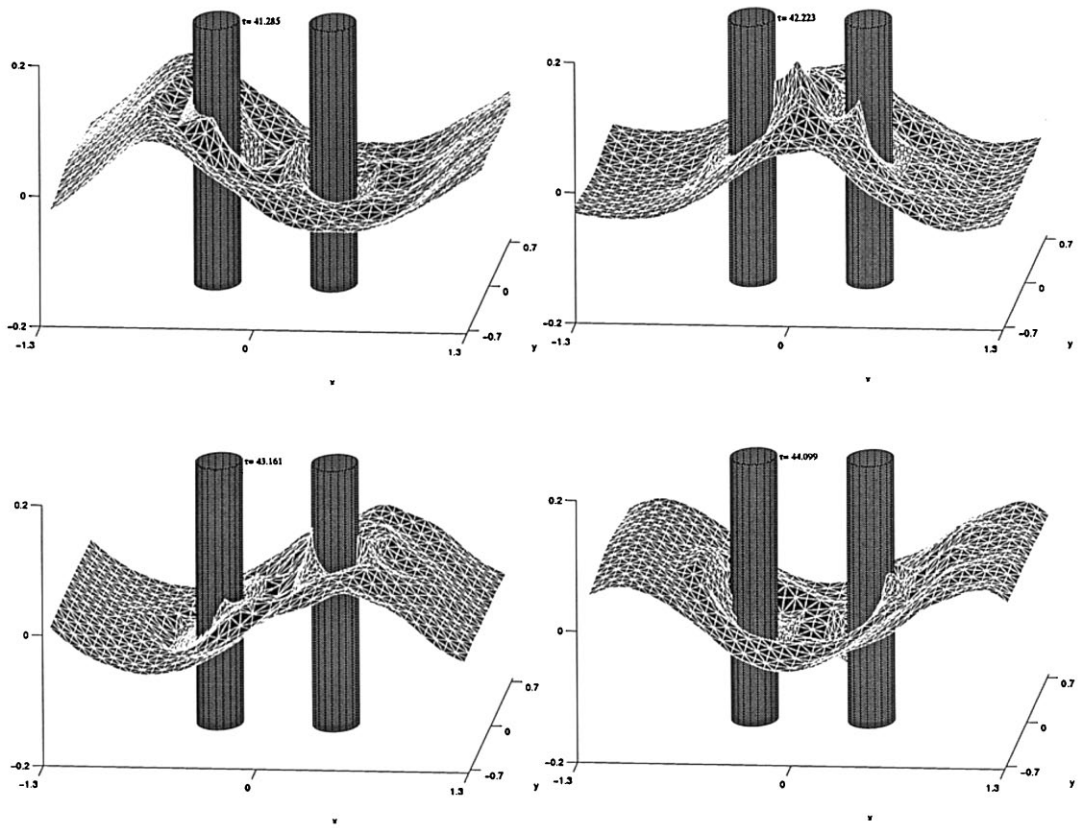

Figure 28. Snapshots of the wave profiles around two cylinders ($kl = 2$, $\omega = 1.6748$, $a = 0.0035$, $R_0 = 0.1416$, $B = 1.416$). Label for x-axis: -1.3, 0, 1.3; for y-axis: -0.7, 0, 0.7; for vertical axis: -0.2, 0, 0.2.

The damping coefficient that is included in the radiation condition described in Part 1 has here been optimized by a series of numerical tests. This method of dealing with the radiation condition has been used in many cases and found to be satisfactory, but our understanding of the reason for this success is far from complete.

Extensive results have been given, including some cases of two cylinders, which are not found in the literature so far. The CPU time used in these cases is roughly of the order of 20 h on a 233 MHz workstation with 96 Mb of memory. This shows that the FEM is quite efficient for dealing with such computationally intensive problem.

ACKNOWLEDGMENTS

This work was sponsored by research grant GR/K80372 from the UK Engineering and Physical Sciences Research Council.

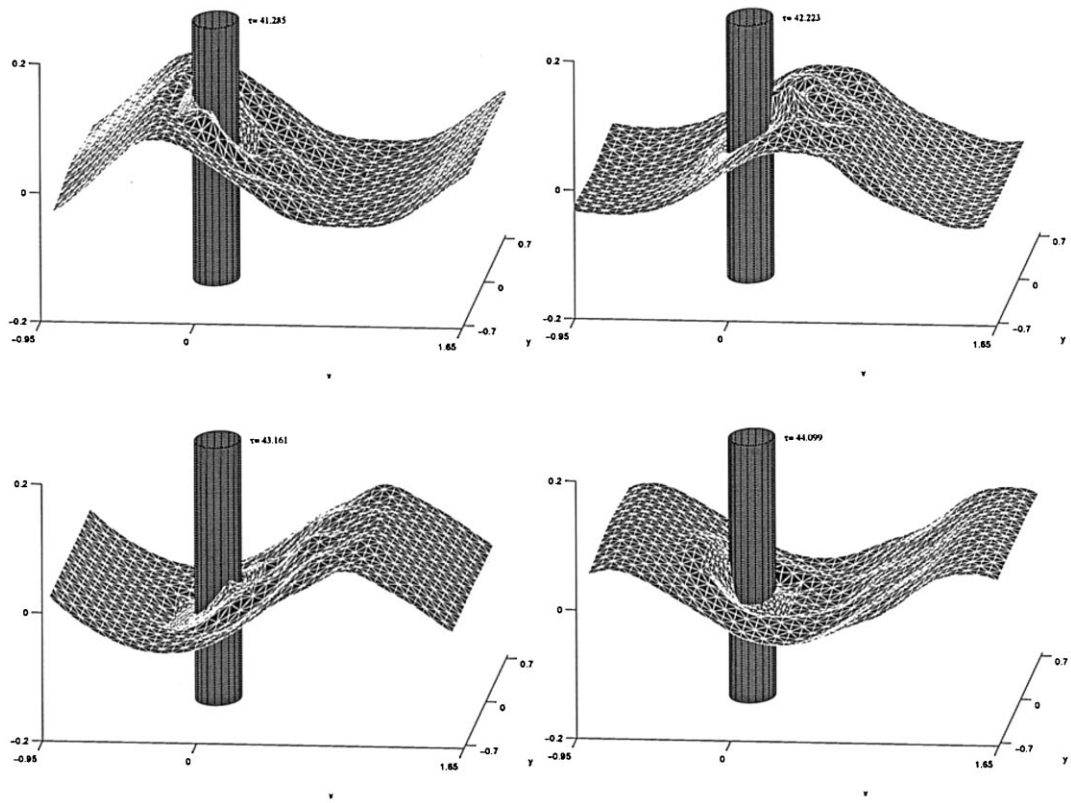

Figure 29. Snapshots of the wave profiles around one cylinder ($kl = 2$, $\omega = 1.6748$, $a = 0.0035$, $R_0 = 0.1416$, $B = 1.416$). Label for x-axis: -0.95, 0, 1.65; for y-axis: -0.7, 0, 0.7; for vertical axis: -0.2, 0, 0.2.

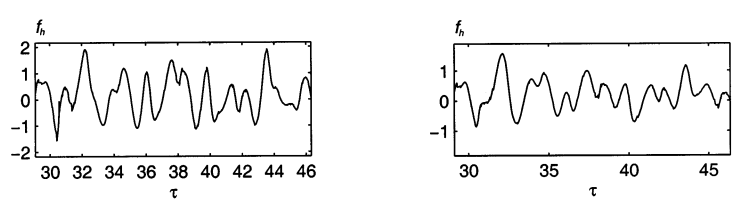

(a) Non-linear force on the first cylinder in the presence of the second one.

(b) Non-linear force on the cylinder without the presence of the second one.

Figure 30. Non-linear contributions to the force acting on the cylinder with or without the interaction between the cylinders ($\omega = 1.6748$, $a = 0.0035$, $R_0 = 0.1416$, $B = 1416$).

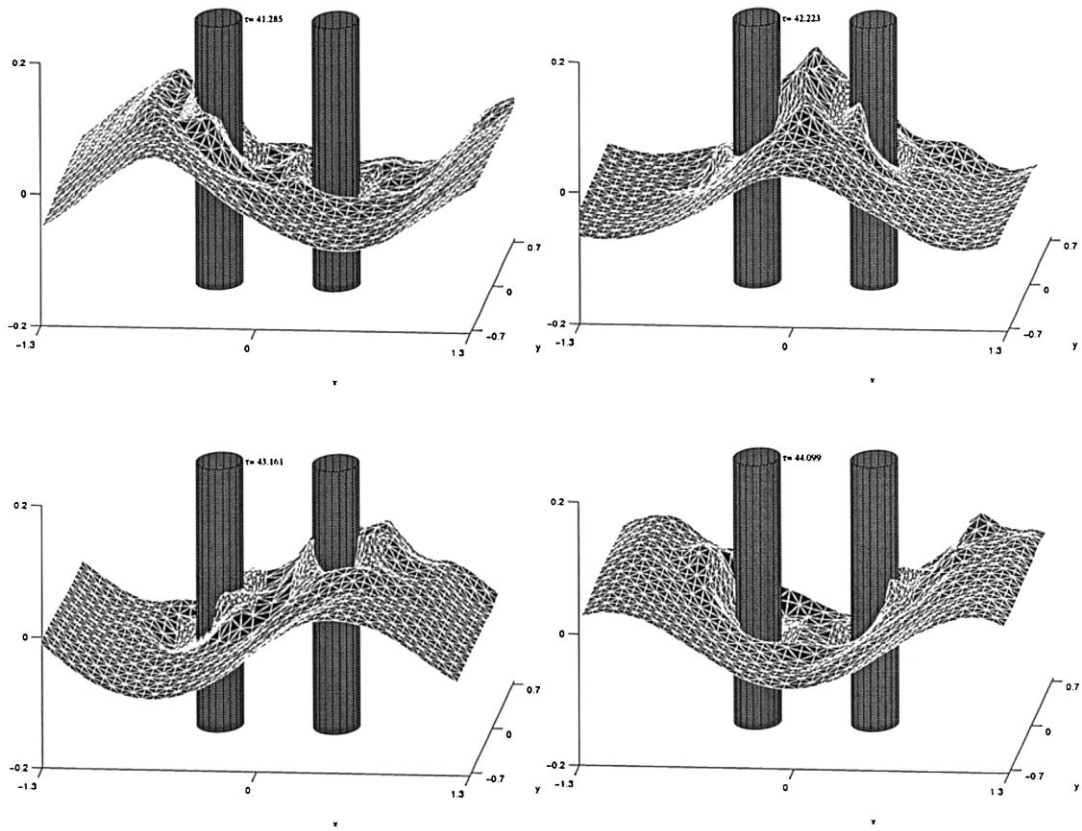

Figure 31. Snapshots of the wave profiles around two cylinders ($kl \approx 2.0$, $l_y \approx 0.3B$, $\omega = 1.6748$, $a = 0.0035$, $R_0 = 0.1416$, $B = 1416$). Label for x-axis: -1.3, 0, 1.3; for y-axis: -0.7, 0, 0.7; for vertical axis: -0.2, 0, 0.2.

REFERENCES

1. Ma QW, Wu GX, Eatock Taylor R. Finite element simulation of fully non-linear interaction between vertical cylinders and steep waves. Part 1: Methodology and numerical procedure. *International Journal for Numerical Methods in Fluids* 2001; **36**: 265–285.
2. Yao Y, Wang P, Tulin MP. Wave groups, wave–wave interaction and wave breaking: results of numerical experiments. In *Proceedings of the 20th Symposium on Naval Hydrodynamics*, Santa Barbara, USA. National Academy Press: Georgetown, SC, 1994; 551–567.
3. Eatock Taylor R, Wang BT, Wu GX. On the transient analysis of the wavemaker. In *9th International Workshop on Water Waves and Floating Bodies*, Kuju, Oita, Japan, Ohkusu M (ed.), 1994.
4. Newman JN. *Marine Hydrodynamics*. MIT Press: Cambridge, 1977.
5. Nestegard A. Status of nonlinear hydrodynamic modelling. Technical report, DNV, Norway, 1999.
6. Clauss GF, Steinhagen U. Numerical simulation of nonlinear transient waves and its validation by laboratory data. In *Proceedings of the 9th International Offshore and Polar Engineering Conference*, Brest, France, 1999; 368–375.

7. Ma QW. Numerical simulation of nonlinear interaction between structures and steep waves. PhD Thesis, Department of Mechanical Engineering, University College London, UK, 1998.
8. Stansberg CT. Experimental local wave pattern around a cylinder. Private communication, 1997.
9. Krokstad JR, Stansberg CT. Ringing load models verified against experiments. *Proceedings of the International Conference on Offshore Mechanics and Arctic Engineering*, *ASME* 1995; **1**: 223–233.
10. McIver P, Evans DV. Approximation of wave forces on cylinder arrays. *Applied Ocean Research* 1984; **6**: 101–107.
11. Malenica S, Eatock Taylor R, Huang JB. Second order wave diffraction by an array of vertical cylinders. *Journal of Fluid Mechanics* 1999; **390**: 349–373.
12. Spring BH, Monkmeyer PL. Interaction of plane waves with vertical cylinders. In *Proceedings of the 14th International Conference on Coastal Engineering*, Copenhagen, Denmark. ASCE: New York, 1974; 1828–1847.
13. Linton CM, McIver P. The scattering of the water waves by an array of circular cylinders in a channel. *Journal of Engineering and Mathematics* 1996; **30**: 661–682.

